RPGR-Associated Retinal Degeneration in Human X-Linked RP and a Murine Model

Wei Chieh Huang,[1] *Alan F. Wright,*[*,2] *Alejandro J. Roman,*[1] *Artur V. Cideciyan,*[1] *Forbes D. Manson,*[†,2] *Dina Y. Gewaily,*[1] *Sharon B. Schwartz,*[1] *Sam Sadigh,*[1] *Maria P. Limberis,*[3] *Peter Bell,*[3] *James M. Wilson,*[3] *Anand Swaroop,*[4] *and Samuel G. Jacobson*[*,1]

Purpose. We investigated the retinal disease due to mutations in the *retinitis pigmentosa GTPase regulator* (*RPGR*) gene in human patients and in an *Rpgr* conditional knockout (cko) mouse model.

Methods. XLRP patients with *RPGR-ORF15* mutations ($n = 35$, ages at first visit 5–72 years) had clinical examinations, and rod and cone perimetry. *Rpgr*-cko mice, in which the proximal promoter and first exon were deleted ubiquitously, were backcrossed onto a BALB/c background, and studied with optical coherence tomography and electroretinography (ERG). Retinal histopathology was performed on a subset.

Results. Different patterns of rod and cone dysfunction were present in patients. Frequently, there were midperipheral losses with residual rod and cone function in central and peripheral retina. Longitudinal data indicated that central rod loss preceded peripheral rod losses. Central cone-only vision with no peripheral function was a late stage. Less commonly, patients had central rod and cone dysfunction, but preserved, albeit abnormal, midperipheral rod and cone vision. *Rpgr*-cko mice had progressive retinal degeneration detectable in the first months of life. ERGs indicated relatively equal rod and cone disease. At late stages, there was greater inferior versus superior retinal degeneration.

Conclusions. *RPGR* mutations lead to progressive loss of rod and cone vision, but show different patterns of residual photoreceptor disease expression. Knowledge of the patterns should guide treatment strategies. *Rpgr*-cko mice had onset of degeneration at relatively young ages and progressive photoreceptor disease. The natural history in this model will permit preclinical proof-of-concept studies to be designed and such studies should advance progress toward human therapy. (*Invest Ophthalmol Vis Sci.* 2012;53:5594–5608) DOI: 10.1167/iovs.12-10070

X-linked retinitis pigmentosa (XLRP) is one of the more severe and common forms of retinal degeneration.[1,2] The retinitis pigmentosa GTPase regulator gene (*RPGR*), accounts for the majority of XLRP.[3,4] Many studies have described the phenotypes in *RPGR*-XLRP, but only one to date has examined the disease course with serial data.[5] Rates of change were estimated for cone-based assays of vision, such as visual acuity, Goldmann kinetic visual field area, and cone flicker full-field electroretinograms (ERGs). A recent study seeking to identify modifier loci among *RPGR*-XLRP patients also collected longitudinal data with functional parameters, but only cone-based flicker ERGs were used to illustrate and grade the phenotypes.[6]

Ocular gene therapy has become feasible as a treatment strategy for inherited retinal degenerations, following reports of safety and efficacy in clinical trials of the autosomal recessive retinal degeneration known as Leber congenital amaurosis, specifically the form caused by mutations in the *RPE65* gene.[7,8] Although there are many hurdles to surmount before treatment of *RPGR*-XLRP can be initiated,[9] the disease is a worthy target because it is a relatively common form of retinitis pigmentosa (RP), and identifiable in the clinic through pedigree analysis and heterozygote detection.[1,10] A major step toward treatment was taken recently with proof-of-concept studies in two canine models of *RPGR*-associated retinal degenerations.[11] At this stage of planning for *RPGR*-XLRP therapy it should be determined what the effects of the disease are, not only on cones, but also on rod-mediated vision. We studied the regional retinal variation of rod as well as cone function in *RPGR*-XLRP patients, and determined how this function changed over years to decades in a cohort of patients.

Another key component for developing therapy relates to availability of disease models that are characterized fully for proof-of-concept studies. Two well-characterized canine models and a number of murine models exist for *RPGR*-XLRP.[12–16] The *Rpgr*-associated diseases in mice that would be amenable to gene augmentation, rather than more complex strategies that assume a dominant negative mechanism, are rather slow and would extend the duration of experiments testing therapies. A novel *Rpgr* conditional knockout (cko) mouse

From the [1]Scheie Eye Institute, Department of Ophthalmology, University of Pennsylvania, Philadelphia, Pennsylvania; [2]MRC Human Genetics Unit, MRC IGMM, University of Edinburgh, Edinburgh, Scotland, United Kingdom; [3]Gene Therapy Program, Department of Pathology and Laboratory Medicine, University of Pennsylvania, Philadelphia, Pennsylvania; and [4]Neurobiology-Neurodegeneration & Repair Laboratory, National Eye Institute, National Institutes of Health, Bethesda, Maryland.

Supported by grants from The Chatlos Foundation, Macula Vision Research Foundation, Hope for Vision, NEI/NIH (EY017549), NEI/NIH (RC3 EY020792), and the NEI intramural research program. AVC is a RPB Senior Scientific Investigator.

Submitted for publication April 22, 2012; accepted July 12, 2012.

Disclosure: **W.C. Huang**, None; **A.F. Wright**, None; **A.J. Roman**, None; **A.V. Cideciyan**, None; **F.D. Manson**, None; **D.Y. Gewaily**, None; **S.B. Schwartz**, None; **S. Sadigh**, None; **M.P. Limberis**, None; **P. Bell**, None; **J.M. Wilson**, ReGenX Holdings (F, C), P; **A. Swaroop**, None; **S.G. Jacobson**, None

Current affiliation: †School of Biomedicine, The University of Manchester, Central Manchester University Hospitals NHS Foundation Trust, Manchester, United Kingdom.

*Each of the following is a corresponding author: Samuel G. Jacobson, Scheie Eye Institute, University of Pennsylvania, 51 N. 39th Street, Philadelphia, PA 19104; jacobsos@mail.med.upenn.edu.

Alan F. Wright, MRC Human Genetics Unit, MRC IGMM, University of Edinburgh, Edinburgh, Scotland, UK; Alan.Wright@igmm.ed.ac.uk.

Investigative Ophthalmology & Visual Science, August 2012, Vol. 53, No. 9

model on a nonpigmented background was genetically engineered, and the results of our analyses of function and structure are compared to those of other models studied to date.

Materials and Methods

Human Subjects

The study included 35 patients with XLRP due to *RPGR* mutations (see Table). Institutional review board approval and informed consent were obtained, and the procedures adhered to the tenets of the Declaration of Helsinki.

Visual Function

Patients underwent a complete eye examination, ERG, visual acuity, and Goldmann kinetic visual fields using previously reported methods.[10,17] Annual rates of change of visual acuity and kinetic visual field extent were calculated separately for each patient by linear regression using longitudinal data. To estimate these rates of change, we used criteria for data censoring similar to those in a previous study of *RPGR*-XLRP.[5] The annual rate of change for the group was obtained by averaging the individual rates.

Static computerized perimetry was performed with 1.7°-diameter, 200 ms-duration stimuli under dark-adapted (500, 650 nm stimuli) and light-adapted (600 nm) conditions. A full-field test of 72 loci on a 12° grid and profiles across the fovea (extending 60° at 2° intervals) were used. Photoreceptor mediation was determined by the sensitivity difference between detection of 500 and 650 nm stimuli.[18,19] Rod and cone sensitivity loss at each test locus was calculated by comparison with normal mean sensitivity at that location under 500 nm, dark-adapted, and 600 nm, light-adapted conditions, respectively. Loci were considered to have no measurable rod sensitivity if loss was >30 dB. Cone-mediated function from dark-adapted perimetry was compared to normal results measured during the cone plateau of dark adaptation. Techniques, methods of data analysis, and normal results for perimetry have been described.[18,19]

Animals

All experiments were performed in compliance with the ARVO Statement for the Use of Animals in Ophthalmic and Vision Research, and the United Kingdom Animals (Scientific Procedures) Act 1986. Animals were born and maintained in controlled ambient illumination on a 12-hour light/12-hour dark cycle (ambient illumination, <3 lux). Access to food and water was ad libitum. Procedures were conducted with approval from the Institutional Animal Care and Use Committee of the University of Pennsylvania.

Generation of Floxed *Rpgr* Mice

A mouse genomic library (a partial Sau3A digest of 129 strain genomic DNA cloned into the BamHI site of the λ2000 vector) was screened with human *RPGR* probes by Southern blotting. A 7kb XbaI fragment was sub-cloned into primer binding site with a modified polylinker and confirmed to contain exons 1 to 4 by Southern blotting with the respective mouse *Rpgr* exons. A loxP site was introduced into the BglII-AvrII fragment 5′ of exon 1 by site-directed mutagenesis (confirmed by sequencing) and sub-cloned back into the 6.5kb genomic clone. A BsaBI site in intron 1 was converted to a SalI site by the use of an oligonucleotide adapter. The genomic clone was linearized with SalI, and an XbaI floxed HSV thymidine kinase-Pgk neomycin resistance cassette, taken from the plasmid 1125 (a gift from Andrew Smith, University of Edinburgh), with SalI adaptors, was inserted to generate the targeting vector pBMR6XLLNTL. The orientation was confirmed by PCR.

The targeting vector was linearized with NotI and electroporated into a male 129 embryonic stem (ES) cell line. Following selection of targeted cells by the addition of G418 to the media, correctly targeted clones were confirmed by Southern blotting using a 507 base pair (bp) probe outside the targeting construct, including part of intron 4, exon 5 and part of intron 5 (PCR primers MusInt4F2 5′ CAGGAGATATGTGCTGTTTAG 3′ to MusInt5R 5′ CAGCGAATGCCTGAATATGC 3′). Targeted clones gave a BglII band of ~4.2 kb compared to a ~7.5 kb wild-type (WT) band.

The HSV thymidine kinase-Pgk neomycin cassette was floxed out by transfecting the targeted clones with pMC-Cre and selecting ganciclovir-resistant clones. To differentiate between the loss of exon 1 and the selection cassette (type I deletion), or loss of the selection cassette only (type II deletion), DNA from the ganciclovir-resistant clones was screened by PCR and sequencing for the presence or absence of the two loxP sites, the neomycin cassette, and intron 1 sequence (3′ loxP site primers ExF6 5′ ATTCTGGGAGCCTTAAATTC 3′ to Mus5′UT-R1 5′ CAAATGTCATTTGCAATCCTAGG 3′ [403 bp]; 5′ loxP site primers MusInt1-F3 5′ GCTGTCCATCGAGTGTCAGC 3′ to MusEx2R 5′ CTGTAACAATAGCAGTATGTTC 3′ [425 bp]; neomycin primers NeoF 5′ GCGATGCCTGCTTGCCGA 3′ to NeoR 5′ GAAGGCGATAGAAGGCGA 3′ [272 bp]; intron 1 primers MusInt1-F4 5′ TTTGGGAATAAATAAATTCCCTTTG 3′ to MusInt1-R4 5′ TTTAAAAGACTTCACGACAGTCAGTC 3′[322 bp]).

Two targeted ES cell clones (E8 and G6) with type II deletions were injected into C57 Bl/6 blastocysts according to standard methods. Line E8 produced one male chimera and line G6 produced two female chimeras, one of which resulted in germline transmission of the floxed *Rpgr* gene.

Homozygous mutant female mice were mated with WT BALB/c male mice purchased from Charles River Laboratories (Wilmington, MA). Male and female heterozygous non-affected offspring then were mated to produce homozygous mutant male and female mice. Genotyping was performed (Transnetyx, Cordova, TN) on DNA isolated from tail snips using a fully automated qPCR-based system targeting the undisrupted WT allele at the 5′ LoxP insertion site by amplifying the following target sequence: CAGGAATGGCATTATTCAACTTGCATGATTGTAATAACATTTATTACGACCATTTATTCAATAAGGATCTAATGTGTGCATCGAGTATATTTGTTTTGTTC as well as targeting the endogenous – LoxP junction site after Cre recombination in the *Rpgr* gene by amplifying this target sequence: AATGGCATTATTCAACTTGCATGATTGTAATAACATTTATTACGACAATAACTTCGTATAGCATACATTATACGAAGTTATTCTAGAGTCGACTCGTTCTAGTCCATCTTATCTTGTCATTGTATATATTTACGTCATATCACTCAAGGAATAGCAC.

Floxed *Rpgr* mice were crossed with transgenic mice ubiquitously expressing Cre under the control of the chicken β actin (CAG) promoter[20] to generate the *Rpgr*-cko mice used in our study.

Genotyping for Conditional Loss of *Rpgr* Exon 1

Genotyping was performed by PCR on DNA isolated from tail biopsies. Floxed mice retaining exon 1 gave a 437 bp amplicon for the PCR ExF6 to Mus5′UT-R1, and mice that had undergone a Cre-induced recombination and were deleted for exon 1 and the flanking sequences, gave a 764 bp amplicon for the PCR ExF6 to MusEx2R.[21]

Optical Coherence Tomography (OCT)

Retinal imaging was conducted as described.[22] Retinal cross-sectional images of control and *Rpgr*-cko mice were acquired with a 3.2 μm resolution SD-OCT system (Bioptigen, Inc., Durham, NC). Animals were anesthetized by intraperitoneal injection (ketamine HCl, 65 mg/kg and xylazine, 5 mg/kg) and pupils dilated topically (tropicamide, 1% and phenylephrine, 2.5%). Corneas were lubricated frequently during the imaging session (Systane Ultra ophthalmic lubricant; Alcon Ltd., Fort Worth, TX). The optic nerve head (ONH) was centered within a 1.6 × 1.6-mm field of view under fast fundus mode, using 200 raster scans of 200 longitudinal reflectivity profiles (LRPs) each. High-

TABLE. Clinical and Molecular Characteristics of the *RPGR* Patients

Patient	Family	Age at Initial Visit (y)	Nucleotide Change	Eye	Visual Acuity*	Refraction†	ERG Amplitude (% of Normal Mean)‡	
							Rod B-Wave	Cone Flicker
P1	F1	7	ORF15+652_653delAG	RE	20/60	−1.50	11	15§
				LE	20/40	−0.50		
P2	F1	10	ORF15+652_653delAG	RE	20/25	−6.00	22	37§
				LE	20/20	−5.75		
P3	F1	19	ORF15+652_653delAG	RE	20/32	plano	19	26
				LE	20/100	−0.50		
P4	F1	25	ORF15+652_653delAG	RE	20/20	−3.00	34	26
				LE	20/20	−2.50		
P5	F1	20	ORF15+652_653delAG	RE	20/20	−3.00	65	26§
				LE	20/25	−2.00		
P6	F1	25	ORF15+652_653delAG	RE	20/60	+1.00	ND	10§
				LE	20/40	plano		
P7	F2	11	ORF15+689_692delAGAG	RE	20/50	−7.50	ND	13
				LE	20/30	−4.50		
P8	F2	23	ORF15+689_692delAGAG	RE	20/70	−3.25	10	20
				LE	20/60	−3.00		
P9	F3	7	ORF15+963G>T	RE	20/25	+1.50	NP	NP
				LE	20/30	+1.50		
P10	F3	18	ORF15+963G>T	RE	20/25	+0.50	10	27
				LE	20/25	+0.50		
P11	F3	56	ORF15+963G>T	RE	20/1250	−1.00	ND	ND
				LE	20/400	−1.00		
P12	F3	56	ORF15+963G>T	RE	20/400	−2.00	38	10
				LE	20/1000	−5.00		
P13	F4	30	ORF15+507G>T	RE	20/30	−0.50	ND	5
				LE	20/30	−0.50		
P14	F4	33	ORF15+507G>T	RE	20/40	−6.50	ND	2§
				LE	20/40	−5.25		
P15	F4	49	ORF15+507G>T	RE	HM	+0.50	ND	ND
				LE	HM	−7.00		
P16	F5	5	ORF15+483_484delGA	RE	20/25	−3.25	24	26
				LE	20/25	−3.25		
P17	F5	14	ORF15+483_484delGA	RE	20/40	−4.25	ND	13
				LE	20/50	−4.75		
P18	F6	9	ORF15+352_460dup	RE	20/30	−0.50	ND	6.5
				LE	20/30	plano		
P19	F7	11	ORF15+474G>T	RE	20/40	+3.50	ND	ND
				LE	20/32	+4.00		
P20	F8	12	ORF15+861G>T	RE	20/32	−4.00	ND	1
				LE	20/32	−3.50		
P21	F9	15	ORF15+652_653delAG	RE	20/40	−1.50	8	6
				LE	20/30	−2.25		
P22	F10	16	ORF15+809delA	RE	20/80	−15.00	NP	NP
				LE	20/30	−11.25		
P23	F11	16	ORF15+631delA	RE	20/200	−11.50	ND	ND
				LE	20/200	−11.00		
P24	F12	20	ORF15+689_692delAGAG	RE	20/50	−1.50	ND	ND
				LE	20/60	−2.00		
P25	F12	32	ORF15+689_692delAGAG	RE	20/400	−7.00	ND	ND
				LE	20/400	−6.00		
P26	F12	43	ORF15+689_692delAGAG	RE	20/400	−2.00	ND	5
				LE	HM	−3.75		
P27	F13	21	ORF15+543_546delGGAG	RE	20/25	−4.70	ND	ND
				LE	20/25	−4.50		
P28	F14	20	ORF15+504_507delGGAG	RE	20/80	−5.50	ND	3§
				LE	20/60	−5.00		
P29	F15	22	ORF15+483_484delGA	RE	20/40	−2.50	ND	2
				LE	20/25	−2.00		
P30	F16	23	ORF15+990G>T	RE	20/25	−4.00	11	6
				LE	20/25	−4.25		
P31	F17	35	ORF15+1192_1211del20 bp	RE	20/125	−7.25	ND	ND
				LE	20/200	−7.00		

Table. Continued

Patient	Family	Age at Initial Visit (y)	Nucleotide Change	Eye	Visual Acuity*	Refraction†	ERG Amplitude (% of Normal Mean)‡	
							Rod B-Wave	Cone Flicker
P32	F18	34	ORF15+689_692delAGAG	RE	20/30	−0.75	ND	5§
				LE	20/30	−0.25		
P33	F19	39	ORF15+652_653delAG	RE	20/32	−7.25	NP	NP
				LE	20/32	−7.50		
P34	F20	49	ORF15+504_507delGGAG	RE	20/200	−3.50	ND	ND
				LE	20/400	−2.50		
P35	F21	72	ORF15+652_653delAG	RE	LP	NP	NP	NP
				LE	LP	NP		

ND, nondetectable; HM, hand motion; NP, not performed.

* Best corrected visual acuity.

† Expressed as spherical equivalents.

‡ ERG result is from eye with best-recorded waveform or average of both eyes if good recordings. Expressed as a percent of normal mean amplitude (rod = 292 μV; cone flicker = 172 μV); 2SD below normal equals 67% for rod b-wave and 60% for cone flicker (Aleman et al.[17]).

§ ERG recorded 1 to 4 years (P1, P2, P5, P6/F1; P14/F4; P28/F14; P32/F18) after first visit.

resolution scans (40 parallel raster scans of 1000 LRP each repeated four times) were acquired along the horizontal (nasal-temporal) and vertical (dorsal-ventral) axes. The eyes then were repositioned by placing the ONH at top or bottom center of the view. High-resolution scans were repeated at these locations for a maximum coverage of 3.2 mm. Each LRP had 1024 samples representing 1160 μm of retinal depth along the z-axis.

Post-acquisition processing of OCT data was performed with commercial software (InVivoVue Clinic software; Bioptigen, Inc.) and custom programs (MATLAB 6.5; MathWorks, Natick, MA). Four repetitions of the high-resolution scans were averaged using the manufacturer's software. Vertical scans with ONH at the center, and those superior and inferior to the center of the ONH were merged by custom programs. The LRPs of the merged OCT images were aligned by manually straightening the Bruch's membrane (BM) and choriocapillaris (ChC) reflection,[23,24] which was defined as the second hyperreflective band from the sclerad side. The outer nuclear layer (ONL), the hyporeflective layer sclerad to the outer plexiform layer (OPL), corresponds to the signal trough delimited by the signal peaks defining the OPL and outer limiting membrane (OLM). ONL thickness was determined in a semiautomated fashion using the samples having maximum slope on both sides of the signal trough.[25] The thickness of the group of structures we termed "OS+" (outer segment+), which is the distance between the trough sclerad to the OLM and the trough vitread to BM/ChC peak, based on the LRP.

Electroretinography

Full field ERGs in mice were recorded as described previously[26] using a custom-built ganzfeld, a computer-based system (EPIC-XL; LKC Technologies, Gaithersburg, MD), and specially-made contact lens electrodes (Hansen Ophthalmics, Iowa City, IA). Mice were anesthetized and pupils dilated as for OCT studies (see above). ERG stimuli included increasing intensities of blue light flashes (–4.2 to –0.4 log scot-cd.s.m^{-2}, 0.3–0.5 log unit steps) in the dark-adapted state (>12 hours). After a two-minute wait, ERG photoresponses were evoked with 2.2 and 3.6 log scot-cd.s.m^{-2} flashes. White flashes of 0.4 log cd.s.m^{-2} on a 25 cd.m^{-2} white background were used to elicit cone function.

Leading edges (4–10 ms, depending on the response) of ERG photoresponses were fit with a physiologically-based model of rod phototransduction activation,[26–29] as they are thought to represent the retina-wide sum of light-induced dark-current shut-off in mouse rod photoreceptor outer segments.[30] The maximum amplitude and sensitivity parameters were derived by minimizing the average root-mean-squared error with a simplex algorithm while holding the remaining parameters constant ($\tau sc = 0.85$ ms; $\tau OS = 0.5$ ms; $\delta = 1.1$ ms)[27]; the fastest photoresponse was assumed to have a saturated amplitude. B-wave amplitudes for white flashes of 0.4 log cd.s.m^{-2} on a 25-cd.m^{-2} white background were used to assess cone function. Age-related rates of decline between these rod and cone ERG metrics were compared by multiple linear regression.[31]

In a subset of the mice ($n = 8$ eyes for *Rpgr*-cko; $n = 4$ eyes for WT), S-opsin- and M-opsin-mediated cone functions were compared using a pair of responses to ultraviolet (UV) and green stimuli presented in the light-adapted state (40 cd.m^{-2} white background) as described previously.[22,32,33] In short, green flashes were produced by an LED source (510 nm peak, 0.87 log cd.s.m^{-2}, 4 ms duration) and UV flashes were obtained from a filtered xenon source (360 nm peak). The intensity of the UV flash was chosen to produce responses matched in waveform to those elicited with the green flash in the WT mice. Both stimuli were presented in a ganzfeld (Espion; Diagnosys LLC, Littleton, MA; Hoya U-360 filter; Edmund Optics, Barrington, NJ) lined with aluminum foil.[34]

Histology

Eyes were fixed immediately after enucleation in 2.5% glutaraldehyde, 2% paraformaldehyde in PBS at room temperature for at least 24 hours, dehydrated with graded ethanol, and embedded in paraffin. Complete sectioning of whole eyes was performed through the vertical meridian from nasal to temporal. Sections (5 μm thickness) were collected at regular intervals from ~24 sites per eye, stained with hematoxylin and eosin, and photographed (Nikon Eclipse Ti-E inverted microscope; Nikon Instruments Inc., Melville, NY). Images from the superior and inferior sides of the ONH were montaged digitally (Adobe Photoshop 6.0; Adobe Systems, San Jose, CA) and straightened (ImageJ, available in the public domain at http://rsb.info.nih.gov/ij/). ONL thickness was estimated by outlining the boundaries of the OPL (sclerad side) and OLM, and measuring their distance at regular intervals of approximately 0.2 mm (Engauge digitizer, ver. 4.1; available in the public domain at http://digitizer.sourceforge.net/). Images from a calibration target (Graticules, Ltd., Tonbridge, Kent, UK) were used to scale the measurements.

Results

Clinical Characteristics of the *RPGR*-XLRP Patients

The 35 patients (ages 5–72 years at first visit) with *RPGR-ORF15* mutations were from 21 unrelated families (see Table). Origins of the patients were European/British in 12 families. The remaining patients were of Ashkenazi Jewish (4 families), Hispanic (3), African-American (1) or Iranian (1) ethnicity. ERGs were recorded in 31 of the patients (see Table). At the

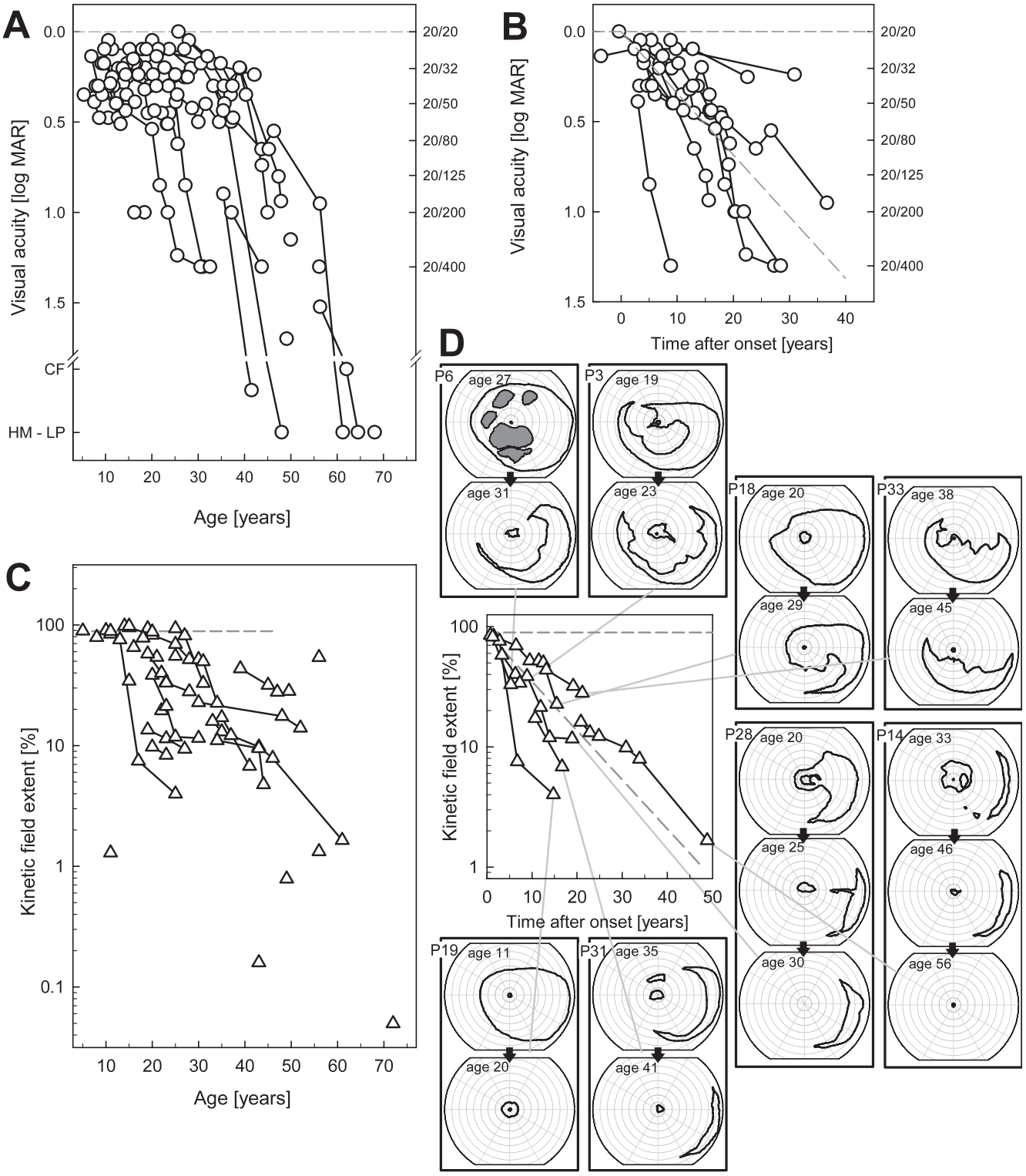

Figure 1. Visual acuity and kinetic perimetry results in *RPGR*-XLRP. (**A**) Visual acuity as a function of age in the entire cohort of 35 patients. Longitudinal data are shown as symbols connected by lines. (**B**) Subset of patients with longitudinal data and follow-up intervals from 3 to 28 years. To compare acuity changes in these patients, data were arranged as time after estimated onset of decline in acuity. *Diagonal gray dashed line through the data*: average of individual slopes. (**C**) Kinetic visual field extent (as % of normal mean) for the V-4e target as a function of age in the entire cohort; longitudinal data shown as symbols connected by lines. (**D**) Subset of patients with longitudinal data (follow-up intervals from 3–28 years) with data arranged as time after onset of decline of field extent. *Diagonal dashed line*: depicts the average of individual decline rates. Examples of kinetic visual field maps (to V- and I-4e targets) are shown at different ages for 8 of the patients (2 or 3 fields per patient are boxed together in the columns surrounding the graph). Patient number and ages are given, and each patient series is connected by *lines to the data on the graph*. Isopters for the I-4e target are interior to the V-4e isopters. *Gray areas*: absolute scotomas. All fields are depicted as right eyes.

earliest visit, 15 patients had no detectable rod and cone waveforms, or no detectable rod or cone ERG and ≤5 μV of signal from the other stimulus (ages 11–56, average, 28). The remaining patients were considered in three ERG categories: 11 patients had more rod than cone dysfunction (ages 9–43, average 21), 3 had more cone than rod dysfunction (ages 20–56, average 34), and 4 had relatively equal rod and cone dysfunction (ages 7–33, average 14). Interestingly, of the 6 family members in F1, 3 had rod > cone dysfunction, 2 had cone > rod dysfunction and one had almost equal dysfunction, thus supporting other such observations.[35]

Visual acuities in this cohort of patients, as measured on the first visit, ranged from 20/20 to light perception (LP; see Table, Fig. 1A). Cross-sectional data analyzed across ages showed a decline with increasing age, as demonstrated previously.[5,36,37] Longitudinal data were available in 18 patients and the follow-up intervals ranged from 3 to 28 years (average 13 years, Fig. 1B). The average of individual slopes indicated a decline in acuity of 8.2% per year. For comparison with previously reported data on visual acuity in *RPGR*-XLRP,[5] the decline in our study is equivalent to 0.079 lnMAR per year.

Kinetic field extent was quantified for the V-4e target[10] and expressed as a percent of normal mean (Figs. 1C, 1D). Cross-sectional data analyses indicated a loss of visual field extent with patient age (Fig. 1C) as noted previously.[5,36,37] To determine the progression of visual field loss in patients, longitudinal data were available in 13 patients with follow-up intervals from 3 to 28 years (average 11 years, Fig. 1D). We assumed a model wherein the disease progresses exponentially after its onset.[38–42] The average of individual slopes indicated a decline in visual field extent of 9% per year For comparison with previously reported kinetic visual field data, this decline is equivalent to 0.094 ln(Extent %) per year.[5,43] Examples of serial kinetic fields are shown to illustrate patterns of loss that underlie the calculated extents. For example, there can be full fields to this target (e.g., P18, age 20; P19, age 11), presence of absolute midperipheral scotomas (e.g., P6, age 27; P18, age 29), and a near complete or complete annular midperipheral scotoma that increases in dimension with age (e.g., P3 ages 19–23; P28 ages 20–25). Annular midperipheral scotoma can increase in dimension with age (e.g., P14 ages 33–46; P31 ages 35–41) and the latest stage of disease could be only a retained small central island without detectable peripheral islands, as in P19 and P14, or only temporal peripheral islands without a detectable central island, as in P28 (each with longitudinal data showing earlier patterns).

Rod Function in the Central Retina of *RPGR*-XLRP can be Normal or Absent

Summaries of the phenotype of XLRP, in general, and *RPGR*-XLRP, in particular, usually describe severe night vision abnormalities in the first decade of life.[1,44] Rod function in *RPGR*-XLRP traditionally has been quantified with full-field ERGs or dark-adapted thresholds at one or more loci.[36,37,45–47] To understand the level of rod (and cone) dysfunction in our patients with *RPGR*-XLRP, we used chromatic perimetry to assess function across the visual field in the dark- and light-adapted states. The first hypothesis we tested was whether there was a simple relationship of amount of central rod-mediated vision with age. Data from 8 patients, 4 of whom have longitudinal measurements, are shown and grouped by age (Figs. 2A–C). Five patients 10 to 13 years old and all with visual acuities between 20/25 and 20/60, have dramatic differences in central rod dysfunction (Fig. 2A). P2, at age 11, has normal levels of rod function in the central 20° while P1, at age 10, retains nearly normal rod function temporal to fixation, but has major loss of rod function nasally. P18 at age 13 has very limited, but detectable rod function in the central field; P19 (age 13) and P20 (age 12) are almost entirely cone-mediated across the region studied (Fig. 2A). Cone sensitivities reach normal levels at the center, and as with rods there is variability within these patients of similar age. The differences in cone function are, however, less pronounced than those observed for rods. Longitudinal data for P18, 12 years later at age 25, showed loss of all rod function centrally; both P19 and P20, 11 to 12 years after the visits shown above, show mainly progression of paracentral cone loss (Fig. 2B, right). In contrast to these cone-only horizontal profiles at ages 23 to 25, P30 at age 23 has normal or near normal rod function in the central 20°. P28 at age 23 has reduced, but detectable rod function in the central field (Fig. 2B). At the end of the third decade of life, P30 has lost considerable central rod function except in the temporal central field, a pattern at age 28 that resembles that in P1 at age 10. A decay in cone function is visible after this 5-year interval, but to a lesser degree than observed for rods. Illustrating further the spectrum of results, P13 at age 30 has normal rod function in the central 20° and a rod pattern similar to that of P2 at age 11 and P30 at age 23; this also applies to cones. These 12 examples indicate a spectrum of rod function loss centrally with no simple relationship to patient age. Follow-up results document the progression and loss of this rod function.

Some patterns of central rod and cone dysfunction (Fig. 2D) did not resemble the other patient data. For example, P16 at age 10 had diffuse rod dysfunction (~1.5 log units) with relatively preserved cone function across the sampled horizontal meridian. P5, at age 42, part of a large family with *RPGR*-XLRP (F1; see Table) that included P1 (Fig. 2A), had normal rod function except at fixation and a diffuse cone sensitivity loss (~<1 log unit), but visual acuity of 20/30. P33, at age 45, had near normal rod function outside of the very central field and there was cone function in a small central island (with visual acuity of 20/40) and some greater cone function detectable further in the periphery. P16 would be considered as having a clinical phenotype of retinitis pigmentosa, while P5 and P33 would likely be categorized as forms of cone-rod dystrophy.[48]

Two Different Histopathologic Patterns from Postmortem XLRP Donor Retinas Compared to In Vivo Measures of Rod and Cone Function Sampled across the Retina

Two studies of eye donor tissue from XLRP patients (one with a known *RPGR-ORF15* mutation) provide a foundation for understanding the detailed photoreceptor disease expression in vivo. One study was of a 24-year-old man with XLRP (presumed, for this situation, to be caused by an *RPGR* mutation).[49] There were mainly cones with outer segments (OS) in the central retina and rods, and cones with OS in the far periphery. Dark-adapted perimetry in two patients (ages 16 and 28) with XLRP showed the same photoreceptor-mediated patterns, and indicated that noninvasive characterization with such methods was feasible and related to underlying histopathology.[50] A very different pattern of disease was documented decades later with the eye donor study of a 69-year-old man with an *RPGR*-ORF15 mutation.[51] There was some maculopathy (visual acuity of 20/60) with perifoveal loss or reduced photoreceptors with abnormal OS. Remaining retina had loss of cones, but not rods.

Were these two patterns present in our cohort of *RPGR*-XLRP patients? Rod and cone sensitivity losses plotted across >70° of visual field[18,19] were available from 30 of the 35 patients. The first histopathology pattern was present in 7 patients at their first visit (at ages 12–35; median age 23).

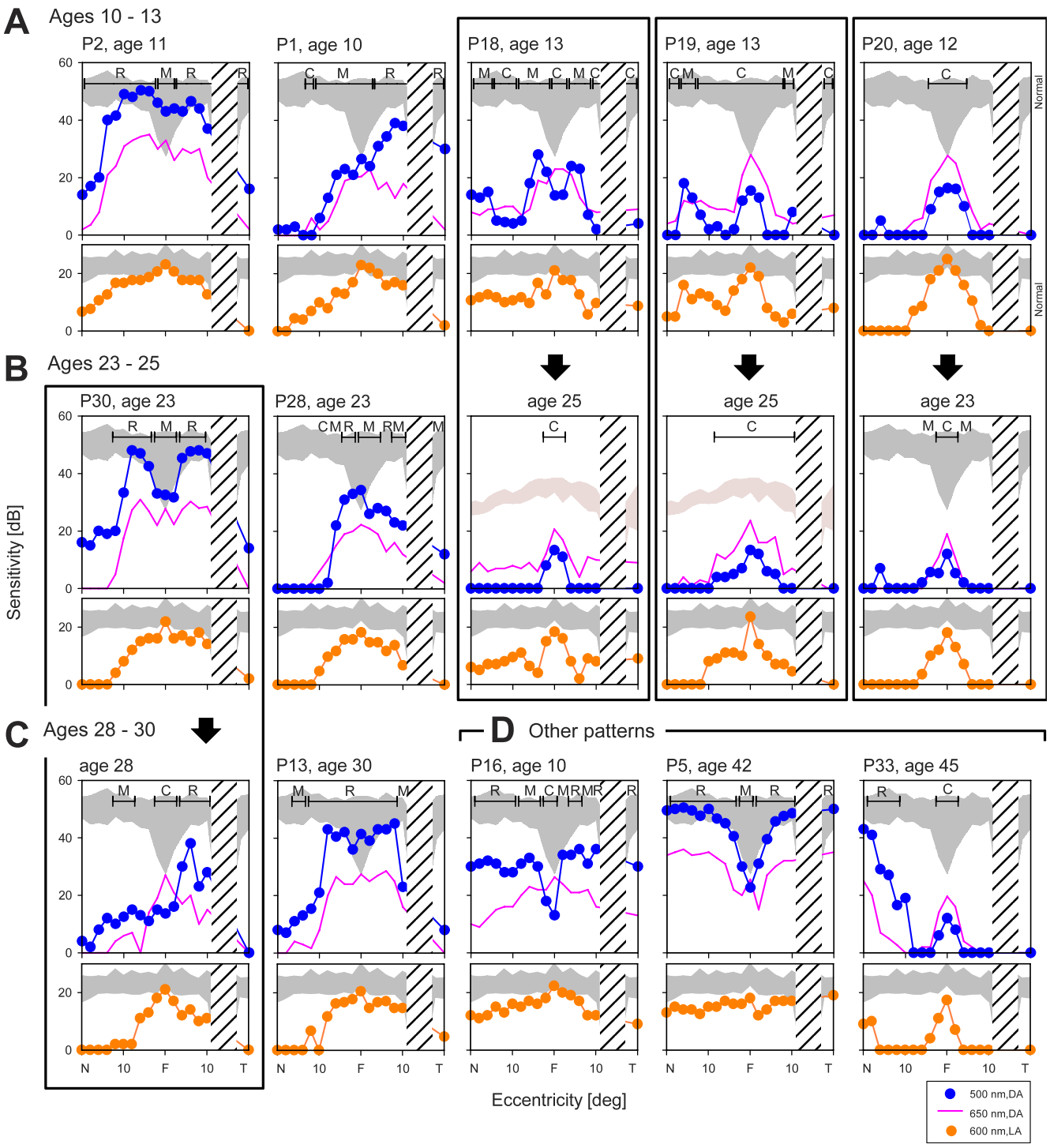

Figure 2. Central rod and cone dysfunction in *RPGR*-XLRP at different ages. Dark-adapted two-color (500 nm, 650 nm) sensitivity profiles across the horizontal meridian (central 40°) in the patients (*symbols* are for 500 nm stimuli; *continuous lines* are 650 nm data) compared to normal (*shaded bands*, mean ± 2 SD, to 500 nm for rod sensitivity). The photoreceptor mediation at loci with function, based on the sensitivity difference between the two colors, is given. R, rod-mediated; M, mixed rod- and cone-mediated; C, cone-mediated. Light-adapted (600 nm) sensitivity profiles are shown for the same patients *below* the dark-adapted data. *Shaded band*: represents normal data (mean ± 2 SD). (**A**) Ages 10 to 13-year-old patients with different degrees of rod and cone dysfunction. (**B**) Ages 23 to 25-year-old patients with similar variations in rod and cone dysfunction as in the younger age group. Note that 3 of the 5 patients in the younger group have serial data (*boxed together in columns*) in their next decade of life and show that some of the residual rod function is lost over this interval (P18, P19, and P20). (**C**) Ages 28 to 30-year-old patients. P13, at age 30 shows normal central rod function and P30, followed longitudinally from age 23 until age 28 (*boxed in a column*), has a reduction in rod function over this interval. (**D**) Other patterns detected in the cohort of *RPGR*-XLRP patients included: a diffuse rod dysfunction at an early age (P16), normal rods and only slightly diminished cones (P5), and relatively preserved midperipheral rod and cone sensitivity, but only a small central island of cone-mediated vision (P33). F, central fixation locus; N, nasal; T, temporal visual field. *Hatched areas*: indicate position of the physiologic blind spot.

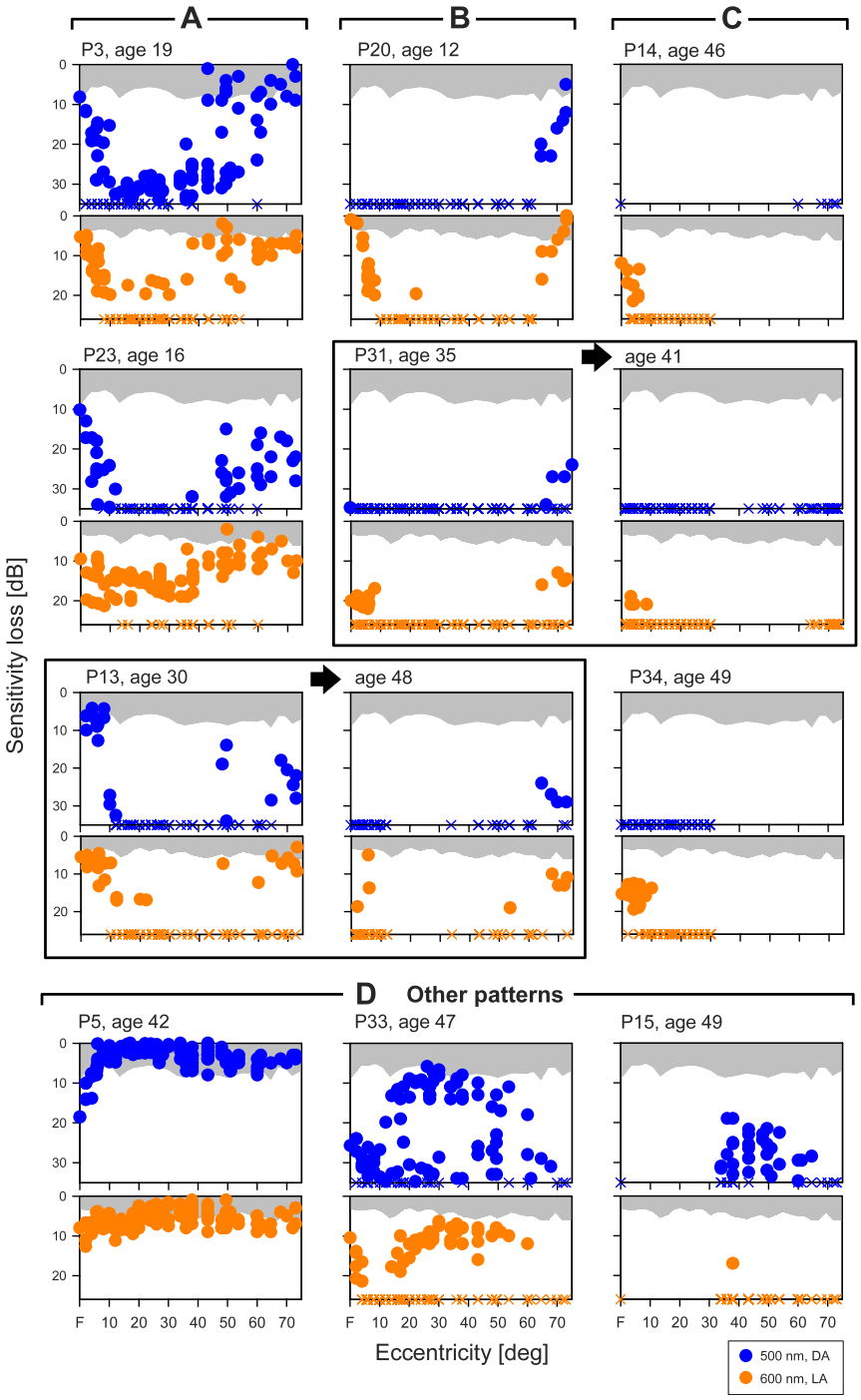

Figure 3. Patterns of rod and cone dysfunction across >70° of visual field in patients with *RPGR*-XLRP. (**A–C**) *Upper panels*: dark-adapted sensitivity loss to the 500 nm stimulus (*filled blue symbols*). *Lower panels*: light-adapted sensitivity loss (*orange filled symbols*) to the 600 nm stimulus. *Shaded bands*: 2 SD limits from normal mean. The data in *column B* are postulated to be the psychophysical correlates to a histopathologic pattern reported previously for an XLRP postmortem donor retina.[49] P20, P31, and P13 have residual central cones, and abnormal peripheral rods and cones. Serial data from P13 (at ages 30 and 48; *boxed together with arrow between*) suggest central rods precede the cone-only central pattern of *column B*. Data, such as those in the patients in *column A* (P3, P23, and P13), are proposed to be the earlier stage of the pattern in *column B*. A cone-only central island with no detectable mid- and far-peripheral function (*column C*) is a more advanced stage than in *column B*; this hypothesis is based on the longitudinal data in P31 (at ages 35 and 41; *boxed with arrow*). (**D**) Other patterns of rod and cone sensitivity losses are illustrated by data from P5, P33, and P15. The patient data are likely to represent different severity stages of the cone-rod dystrophy phenotype of *RPGR*-XLRP, which also has been documented in postmortem donor retina.[51] F, central fixation locus.

Examples of this pattern are P20 (age 12), P31 (age 35), and P13 (age 48, second visit, Fig. 3B). All have preserved central cones as well as peripheral rod and cone sensitivity, separated by a midperipheral scotoma. Longitudinal data in two of the patients, P13 and P31, provided insight into the natural history of this disease expression. P13 at age 30 (first visit) had measurable and near normal central rod sensitivity. Eighteen years afterward, this central rod function was lost and

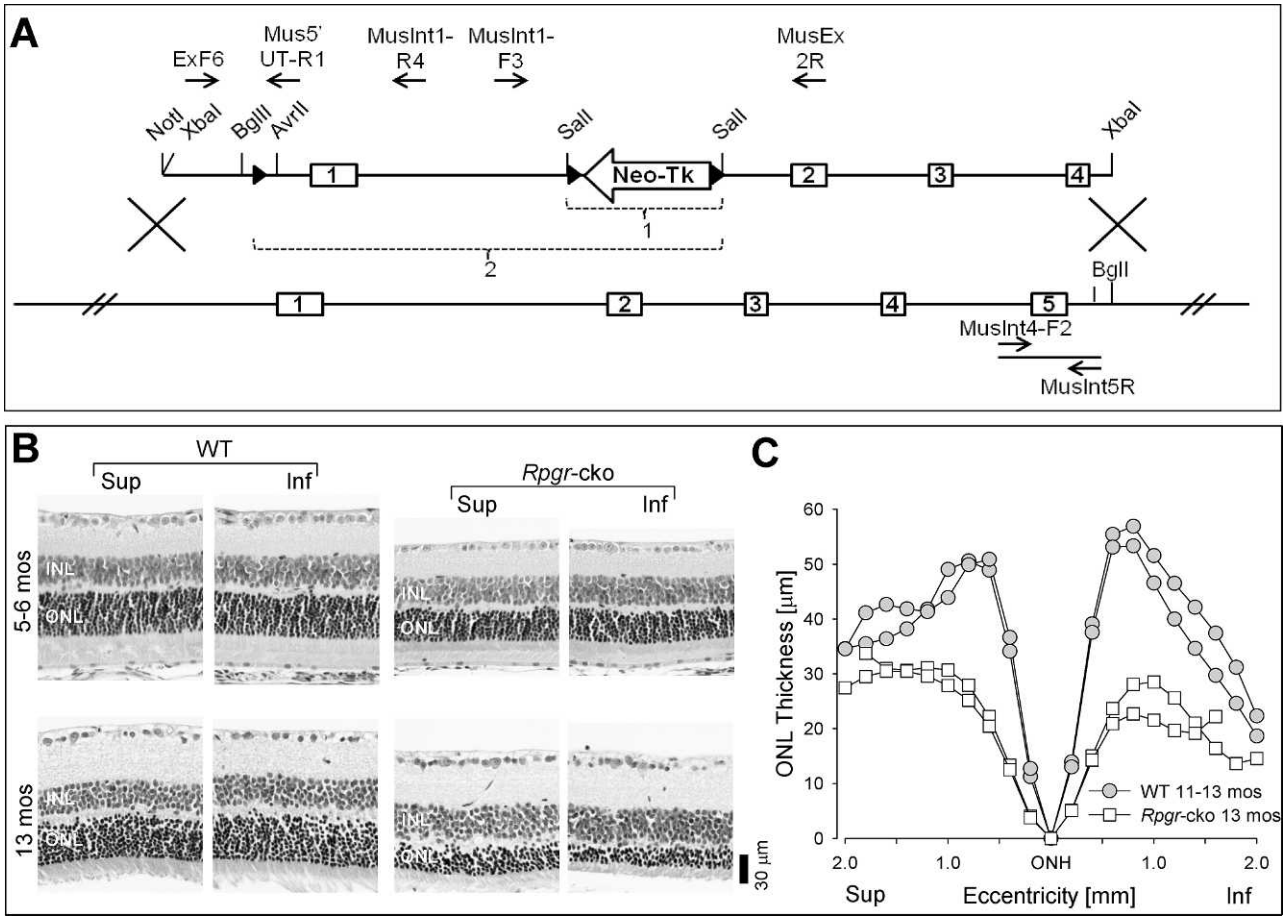

Figure 4. *Rpgr*-cko mouse: genetic engineering and retinal histopathology at early and late ages. (**A**) Generation of *Rpgr*- cko mouse is illustrated with a cartoon of the targeting construct pBMR6XLLNTL (*top*) and the WT *Rpgr* locus (*bottom*). The *Rpgr* proximal promoter region and exon 1 are deleted (*bracketed region labeled* "*2*"). (**B**) Dorsal-ventral (superior-inferior) retinal sections in WT mice at two ages (5–6 and 13 months) compared to similar-aged *Rpgr*-cko mice. Inferior and superior retinal sections are illustrated for each age. Retinal sections are labeled for inner nuclear layer (INL) and ONL. (**C**) ONL thickness as a function of eccentricity along the vertical meridian crossing the ONH in WT ($n = 2$) and *Rpgr*-cko ($n = 2$) mice at the later ages (11–13 months). Sup, superior; Inf, inferior retina.

peripheral sensitivities decreased. Other examples of this pattern are P3 at age 19 and P23 at age 16 (Fig. 3A); a total of 11 patients showed this pattern at first visit (ages 10–30; median age 16).

P31 at age 41 indicates that disease progression can lead from the first histopathologic pattern (Fig. 3B) to central cone function only and no detectable peripheral sensitivity. Further examples of this more advanced disease stage are P14 at age 46 and P34 at age 49 (Fig. 3C). A total of 4 patients showed this pattern of a cone-only central island without extracentral detection of rod or cone stimuli at their first visit (ages 21–56, median age 41).

The second histopathology pattern is exemplified by P15, at age 49, who showed some preserved mid- and far-peripheral rods, but little or no measurable cone function (the "cone-rod dystrophy" phenotype[51]). Two other patients may provide a view of earlier stages of this disease expression. P33, at age 47 years, had measurable, but reduced rod and cone function across most of the field with many loci retaining rod (and cone) function in the mid-periphery. P5, at age 42, could represent very early expression with rod sensitivity loss only near fixation, and a diffuse, albeit mild, cone dysfunction across the field (Fig. 3D). It is of interest that P5, at first visit at age 20 years, had rod and cone sensitivities that were within normal limits by these measures.

Other patterns could not be fit into a sequence involving the first or second histopathologic patterns. Three patients had all cone-mediated fields or a diffuse loss of rod function with near normal cone function across the field (P16–P19, ages 10–12). Two other young patients had substantial rod and cone function in the central field, but no detectable peripheral function (P1 at age 7, and P7 at age 10). All 5 of these patients eventually could progress to cone central islands only, such as we hypothesized would be the end stage of the first histopathologic pattern.

Rpgr-cko Mouse Model of *RPGR*-XLRP

A conditional *Rpgr* knockout mouse (*Rpgr*-cko) was generated; the targeting construct pBMR6XLLNTL (top) and the WT *Rpgr* locus (bottom) are illustrated (Fig. 4A). Three loxP sites were engineered in to pBMR6XLLNTL, one in the 5′ UTR and two flanking the neomycin-thymidine kinase cassette in intron 1. The selection cassette was floxed out by transfecting targeted ES cells with pMC-Cre (bracket labeled "1"). The *Rpgr* locus was knocked out in floxed mice by crossing them with a transgenic mouse ubiquitously expressing Cre under the

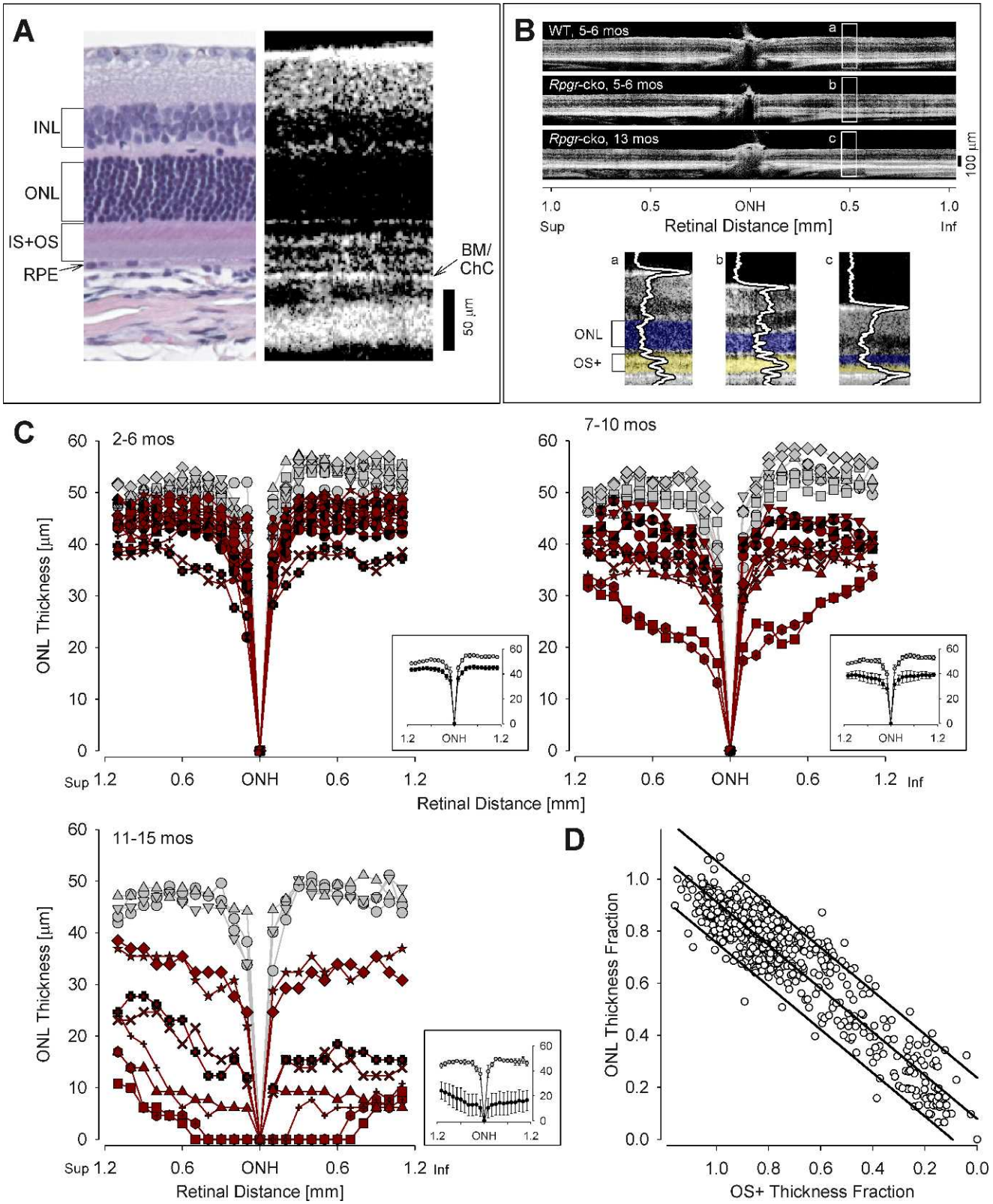

Figure 5. OCT abnormalities in *Rpgr*-cko mice. (**A**) Comparison of histologic and OCT sections in WT BALB/c mice illustrates the lamination patterns that appear with noninvasive optical imaging (4 months old, histologic section; 5 months old, OCT scan). BM/ChC, Bruch's membrane/choriocapillaris; IS+OS, inner segments +outer segments. (**B**) Representative OCT scans (*top*) across ~2 mm of retina centered at the ONH, to illustrate ONL thickness changes with age in *Rpgr*-cko mice. Images from the inferior retina were magnified and overlaid with LRPs to demonstrate the reflective abnormalities in the outer retinal region in *Rgpr*-cko mice (**b, c**) compared with WT (**a**). OS+ is defined as the distance between the hyporeflective trough which is sclerad to OLM and the hyporeflective trough which is vitread to BM/ChC peak. (**C**) Superior-inferior OCT sections were quantified for ONL thickness in three age groups of *Rpgr*-cko mice (*red symbols*) and age-related WT mice (*gray symbols*). *Insets*: at lower

right of each plot shows the mean ± 2 SE of the data. In the 2 to 6 months age group, 18 *Rpgr*-cko and 10 WT eyes were analyzed; in the 7 to 10 months age group, 12 *Rpgr*-cko and 8 WT eyes were analyzed; and in the 11 to 15 months age group, 8 *Rpgr*-cko and 4 WT eyes were analyzed. (**D**) ONL thickness fraction (locus and age specific) plotted as a function of OS+ thickness fraction. *Graph*: shows a linear relationship (with 95% prediction intervals) of photoreceptor nuclear loss and distal photoreceptor structure loss in *Rpgr*-cko mice ($r^2 = 0.89$, $P < 0.001$).

control of the CAG promoter (bracket labeled "2"). The *Rpgr* gene was deleted for exon 1 and flanking sequences, including predicted transcription start sites and proximal promoter region.[21] The relevant restriction endonuclease sites and PCR primers are indicated (Fig. 4A).

Retinal histology was studied at early (5–6 months) and later (13 months) ages, and compared with histology from WT BALB/c mice of similar ages (Fig. 4B). Sections from superior and inferior retina of WT and *Rpgr*-cko mice suggested some thinning of the ONL in the mutant at 5 to 6 months of age, but more pronounced thinning at 13 months. Some altitudinal differences (inferior ONL thickness less than superior) are observed in the sections from the 13-month-old mutant. Measurements of ONL thickness across 4 mm of retina along the vertical (dorsal-ventral) meridian through the ONH are plotted for older mice (Fig. 4C). There are differences in ONL thickness between WT and mutant across most of the sampled retina and some altitudinal asymmetry with inferior thinner than superior retina in the mutant only (Fig. 4C).

In Vivo Structure in *Rpgr*-cko Mice

To gain further understanding of the progress of retinal degeneration with age, OCT scans were performed in *Rpgr*-cko (ages 2–15 months) and compared to those of BALB/c WT mice of similar ages (Fig. 5). The relationship of retinal histology to OCT reflectivity is illustrated (Fig. 5A). The vitreoretinal interface is hyperreflective, and there are hyporeflective zones corresponding to the INL and ONL; hyperreflective regions deep in the outer retina have been shown to represent IS/OS, RPE, BM, and choroid.[52,53] Representative OCT vertical scans across the ONH show retinal lamination in a WT mouse and in two mutant mice of different ages (Fig. 5B). Magnified images at 0.5 mm inferior retina show thinned ONL in the mutants at 5 to 6 (b) and 13 months (c) compared to the WT sample (a). Also, features of the scan deep to the ONL show differences between mutant and WT: there is loss of discrete lamination between the OLM and BM/ChC in the mutant mice and thinning of this region in older mutants. A similar OCT feature has been noted previously in patients with the *CEP290-NPHP6* and *IQCB1-NPHP5* forms of Leber congenital amaurosis.[33]

ONL thickness was measured across the vertical meridian in 38 eyes of *Rpgr*-cko mice and 22 WT eyes, spanning an age range from 2 to 15 months (Fig. 5C). The data were divided into three age groups: 2 to 6, 7 to 10, and 11 to 15 months. There is considerable variation within each age group, but, in general, there is progressive reduction in ONL with age in the mutants. Mean ONL thickness in *Rpgr*-cko eyes (insets) is lower in all age groups studied compared to that of the age-related WT eyes. Certain regional variations in ONL thickness loss were observed in the mutant data. There was a tendency for parapapillary loss of ONL with increasing disease; only in the oldest age group was there an observed difference between superior and inferior ONL thickness. Our anecdotal observations of thinned outer retinal structures deep to the ONL in the mutant mice, presumed to be mainly photoreceptor IS and OS (Fig. 5B), were supported by measurements of the laminae (Fig. 5D). There was a linear relationship of photoreceptor nuclear loss and distal photoreceptor structure (termed OS+) loss in *Rpgr*-cko mice ($r^2 = 0.89$, $P < 0.001$).

Rod and Cone Function in the *Rpgr*-Mutant Mice

ERG waveforms are shown for representative WT and *Rpgr*-cko mice at two different ages: 5 to 7 and 11 to 13 months (Fig. 6A). At 5 to 7 months of age dark-adapted ERGs in response to increasing intensities of light stimuli in the *Rpgr*-cko mouse do not appear remarkably different from WT at threshold (to the dimmest lights), but amplitudes are reduced at higher stimulus intensities. At 11 to 13 months, the mutant shows some threshold elevation compared to WT, and ERG amplitudes are reduced further at all intensities. Cone ERGs at both ages (Fig. 6A, lower waveform) are reduced in the mutant compared to WT and at the older age, there is no detectable cone ERG in the mutant.

Leading edges of the dark-adapted ERG photo responses are well fit with a model of rod phototransduction activation (Fig. 6B). Compared to WT recordings, *Rpgr*-cko mice had ERG photo responses with reduction of maximum amplitude at both ages represented and there is greater reduction at the older age.

Rod and cone ERG data in all WT and *Rpgr*-cko mice studied were plotted as a function of age (Fig. 6C). The rod photoresponse amplitude ($P3_{max}$) in *Rpgr*-cko mice declines with age and can be described with a log-linear function with a negative slope ($\log_{10}[P3_{max}] = 2.71 - 0.072 \times age\,[months]$; $r^2 = 0.46$). There is little or no reduction of rod amplitude with age in the WT mice. Cone amplitude in WT mice also is stable with age whereas the *Rpgr*-cko mice showed a decline of function with age that also could be well described with a log-linear function ($\log_{10}[P2_{80}] = 1.70 - 0.059 \times age\,[months]$; $r^2 = 0.48$). The slopes of rod and cone function decline were not significantly different ($P = 0.44$).

The histopathologic and some OCT data from *Rpgr*-cko mice suggesting inferior more than superior retinal abnormalities led to the comparison of ERGs of short-wavelength-sensitive (S-) and middle-wavelength-sensitive (M-) cone function. UV and green flashes in the light-adapted state did not show significant mismatches in the *Rpgr*-cko mice compared to the WT group (UV-green difference [SD]: 3 [6.8] μV in *Rpgr*-cko, −2 [10.5] μV in WT, $P = 0.34$). This suggests that the altitudinal pattern of ONL thickness was not accompanied by detectable functional differences.

Discussion

Human *RPGR*-XLRP Phenotype: Interpretable Differences between Patients

XLRP in general and *RPGR*-XLRP in particular are acknowledged to be more severe than many forms of RP.[5,36,44,47] Visual acuity and kinetic visual field results from our study concur in general with those of previous studies that quantified rates of decline of function in XLRP.[5,36,37] The complexity of phenotype with differences in rod and cone disease presentation between patients of different families or even between family members was found in the current cohort, as in previous studies.[6,35,37,54] Given recent progress toward gene therapy in *RPGR*-XLRP with success at treating canine models,[11] there is now a need to reckon with the differences in disease expression between patients and devise a plan for therapeutic intervention. We chose to begin by using a framework to divide

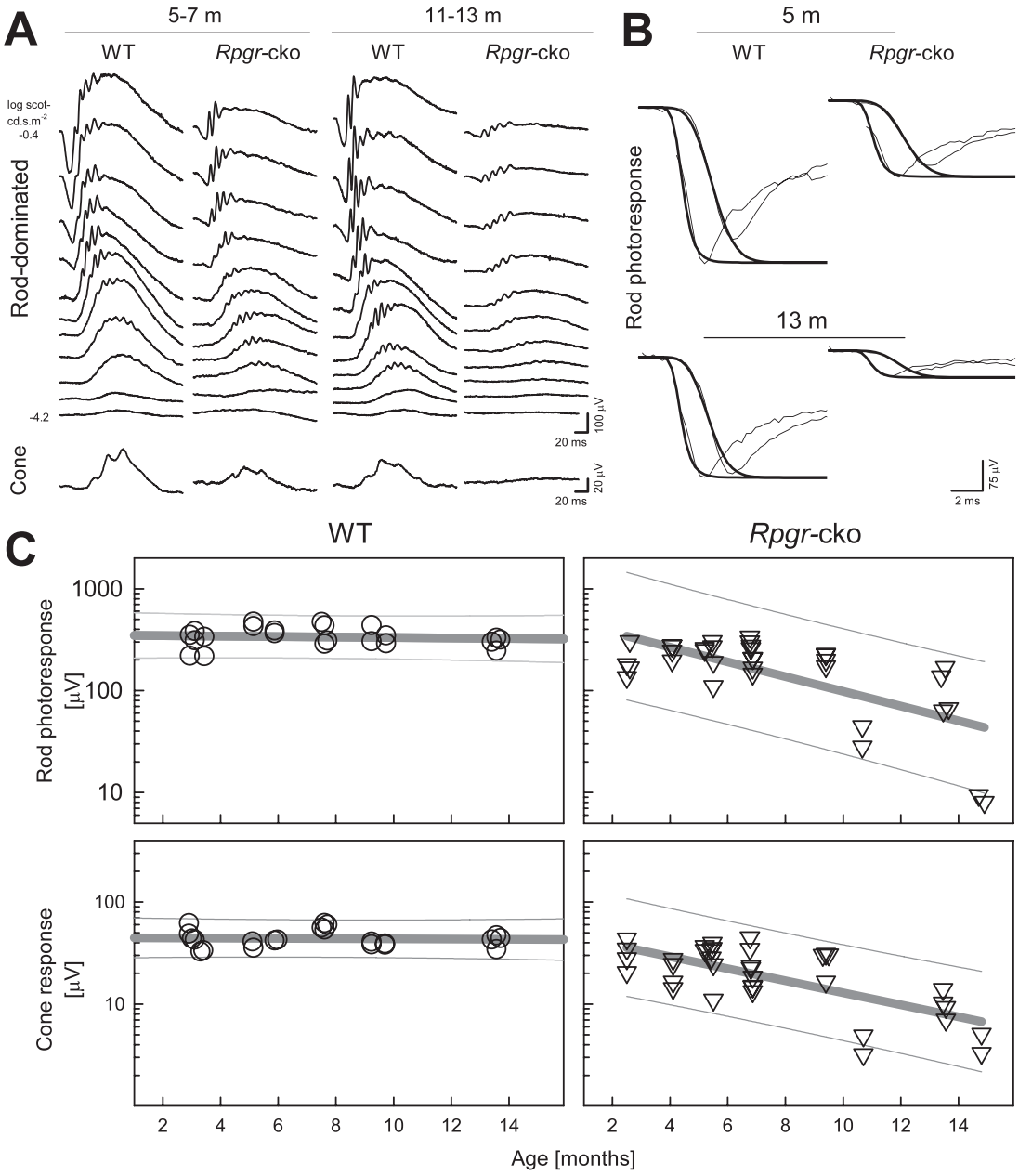

Figure 6. Retinal function change with age in *Rpgr*-cko mice. (**A**) Dark-adapted ERG luminance-response series (*upper set of waveforms*) over a range from −4.2 to −0.4 log scot cd.s.m^{-2} blue flashes. There are reduced amplitudes to higher intensity stimuli in *Rpgr*-cko mice compared to WT waveforms at the ages of 5 to 7 and 11 to 13 months. ERG amplitudes are reduced in the older *Rpgr*-cko mouse compared to the younger mouse. Cone ERGs (*lower row of waveforms*) also show substantial abnormalities in amplitude. All traces start at flash onset. (**B**) Leading edges of dark-adapted ERG photoresponses evoked with 2.2 and 3.6 log scot cd.s.m^{-2} flashes (*thin traces*) fit as an ensemble with a model of rod phototransduction activation (*thick traces*). Representative results are shown for two ages. Note the substantially smaller responses from *Rpgr*-cko mice. (**C**) *Top*: rod photoreceptor function estimated with the maximum amplitude parameter of ERG photoresponses over the ages from 2 to 15 months in WT (*left*) and *Rpgr*-cko (*right*) mice. *Below*: Cone ERG amplitude as a function of age. Regression lines (*thick gray*) describe log-linear change of the parameters with age; 95% prediction intervals (*thin gray lines*) encompassing the data are also shown.

phenotypes that draws from results of the only two postmortem retinal histopathology studies. These studies showed major differences in regional variation of the disease and very different effects on rod compared to cone structure and function.[49,51] The phenotype defined by the histopathology report 30 years ago[49] was detectable by two-color dark-adapted perimetry, a technique used in our study.[50] This phenotype, associated previously with XLRP of unknown genotype, is now confirmed in our study to be the common pattern in *RPGR*-XLRP. The second phenotype was identified in the present cohort in a few patients using the same psychophysical method. Our cross-sectional data with some longitudinal studies indicated that most patients can fit within the framework of the two histopathologic patterns.

The more common phenotype in our cohort of *RPGR*-XLRP patients by rod and cone psychophysics[49,50] showed cone-mediated central islands separated from peripheral rod and cone islands by a midperipheral scotoma. Using our longitu-

dinal data in patients, we concluded that this phenotype was preceded by stages with detectable or near normal central rod function, and succeeded by stages with only residual cone central islands and no detectable peripheral function. We propose that this sequence is the main one in *RPGR*-XLRP and patients can be categorized by whether they are in one of these three disease stages. There was no predictable age relationship to the different stages of central dysfunction. Even in the first decade of life, there was variation in the amount of detectable rod function centrally, and such variation was found into the third and fourth decades (Fig. 2).

Our current data also provided rod and cone psychophysical evidence to support the occurrence in vivo of the less common histopathologic pattern[51] with relatively preserved midperipheral function and cone sensitivity more impaired than that of rods. Paracentral losses of function (e.g., P33, age 45; Fig. 2) appear to isolate small central islands of cone function, which may be maintained until late in the disease or lost early. Visual acuity, thus, is not a certain marker for this phenotype although it has been labeled as a cone-rod dystrophy and, by implication, would be assumed to affect acuity early.

Developing a Treatment Strategy for *RPGR*-XLRP

What would be the treatment strategy for the common phenotype, assuming a subretinal mode of gene therapy delivery as used in our *RPE65*-LCA clinical trial and others?[7,8] Targeting the central and far peripheral retina with a two-injection strategy, as we did in later cohorts of our *RPE65*-LCA trial,[8] would seem worth considering. Attention should be paid to the degree of rod as well as cone dysfunction in the central field. Unresponsive peripheral field using chromatic dark-adapted perimetry should be tested with achromatic dark-adapted perimetry as a screening procedure for persistent peripheral islands that have high thresholds. The wider dynamic range of intensities available with achromatic dark-adapted perimetry has been useful to detect function in patients with markedly reduced vision.[55] What would be the expectations with therapy? Early trials primarily would be for safety, so monitoring central and peripheral islands perimetrically for rod and cone function should detect negative functional change. Our previous work in forms of RP and Usher syndrome provides metrics and inter-visit variability for dark- and light-adapted threshold testing.[19] Detecting positive functional change would depend on a better understanding of the relationship between residual function and correlative structure. This was not attempted in our study, but is needed. OCT analyses of the central retina and the relationship of photoreceptor structure to photoreceptor-mediated function will be key to decide the effects of treatment. Given the results indicating treatment efficacy in canine *Rpgr* mutants,[11] efficacy in the short-term in human *RPGR*-XLRP may be in the form of structural change in the OS layer and accompanying increase in rod or cone sensitivity. A comparison of inner retinal OCT abnormalities[56] inside and outside the treated zone[11] also would be worthy outcomes for assaying efficacy. The knowledge of detectable short-term loss and recovery of OS structural parameters after subretinal injections provides useful background information about timing post-treatment of such measurements.[8]

Continuing to assume a two-injection strategy for the second and less common phenotype, placement of a central subretinal injection would be warranted unless there was neither photoreceptor structure nor function detectable in a wide expanse of the macula. An injection in central or pericentral retina and another in adjacent midperipheral retina, where there is a tendency for greater preservation of function, would seem logical to determine safety and efficacy.

Murine Models of XLRP: A Comparison

Several *Rpgr* mutant rodent models have been investigated to date. In addition to the pursuit of greater understanding of the disease mechanism, the models can provide opportunities for proof-of-concept studies that may advance therapeutic interventions relevant to human *RPGR*-XLRP. Reported models differ in genotype and background strain, with phenotypes showing different degrees and time courses of structural and functional losses. Available data on the disease expression for several of these rodent models are summarized (Supplementary Table S1, http://www.iovs.org/lookup/suppl/doi:10.1167/iovs.12-10070/-/DCSupplemental). The naturally-occurring *rd9* mouse shows a relatively moderate disease phenotype, with ERGs decreasing to 60 to 70% of normal at 3 to 5 months, 50% at 11 to 16 months, and 35% at 24 months of age.[57] A genetically-engineered *Rpgr-null* mouse[12,14,58] showed moderate degeneration, with dysfunction reaching 69 to 75% of normal levels at 6 months of age. ONL loss of approximately 50% was observed at 24 months of age. Addition of a mutant ORF15 transgene[14] to the *Rpgr-null* mouse produced a severe disease phenotype with rod ERGs decreasing to 10% of normal levels, and 50% of structural loss 40 days after birth. The faster degeneration rate in this model has been attributed to a gain-of-function mechanism.[14] A different ORF15 transgene was introduced into the *Rpgr-null* mouse, resulting in preservation of ONL thickness and partial recovery of visual function when compared to WT at 14 months of age.[58] The addition of transgenes causing overexpression of two otherwise normal *Rpgr* variants (mRDef, $Rpgr^{ex1\text{-}19}$ and mRORF, Rpgr-ORF15) to the *Rpgr-null* mouse produced either a severe degeneration in the first variant (ONL reduction to 22% of normal by 3–5 months), or the preservation of ONL thickness with possible rescue of the phenotype for the second (no loss observed up to age 3–5 months; the mRORF transgene also was reported not to be deleterious when applied to a WT background). The faster degeneration in the mRDef model was postulated to be related to abnormal accumulations of $Rpgr^{ex1\text{-}19}$ in the photoreceptor outer segment.[16] An exon 4 knockout was engineered and introduced to mice on either BALB/c ($Rpgr^{\Delta Ex4}$ BALB/c) or C57BL/6 ($Rpgr^{\Delta Ex4}$ BL/6) backgrounds by another group,[15] resulting in relatively milder degeneration rates. A difference in phenotype also was found to correlate with the mouse background strain; the $Rpgr^{\Delta Ex4}$ BALB/c showed a comparatively faster cone degeneration rate by ERG, reaching ~40% of normal levels by 12 months of age, but no detectable structural loss, whereas the $Rpgr^{\Delta Ex4}$ BL/6 showed some reduction of ONL thickness, reaching a level of ~85% of normal at 12 months of age. The exon 1 conditional knockout on a BALB/c background presented in our study showed progressive retinal degeneration and visual function loss, and the data suggest a faster degeneration rate than the moderate models described previously. By ~6 months of age, rod and cone ERGs showed a reduction of ~40% compared to normal levels. ONL thickness (by SD-OCT) was reduced to 35% of WT at ~13 months. Cone and rod ERG amplitude reduction as well as structural loss appear faster than in the reported data for the $Rpgr^{\Delta Ex4}$ BALB/c model and without evidence of cone more than rod dysfunction (Supplementary Table S1, http://www.iovs.org/lookup/suppl/doi:10.1167/iovs.12-10070/-/DCSupplemental).

Rpgr-cko Mouse on BALB/c Background: Planning Proof-of-Concept Studies

Recent success in gene augmentation therapy of two natural-occurring *RPGR*-XLRP canine models[11] and phenotype rescue in a zebrafish model[59] present opportunities for further proof-of-concept studies, such as the introduction of a normal *Rpgr* gene to certain *Rpgr* mouse mutants. A monocular interven-

tion intended to halt disease progression in the treated eye while the disease progressed in the untreated eye would require an interocular comparison of function or structure at some time point after the intervention. The minimal waiting period for treatment effect to be detectable under such designs depends on the animal model, the rates of change of structural and functional parameters, and the variability of the measurement paradigm. We have provided data that would enable this estimate to be made in the *Rpgr*-cko model. Assuming known levels of interocular variability in mouse ERG recordings[26] and rates of change (Fig. 6), treatment effect could be detected in the present model by interocular comparison of ERGs at 4 to 6 months after intervention. Outcomes from therapeutic intervention in rodents could be used to estimate treatment efficacy, paving the way to early stage therapeutic trials for human XLRP at different disease stages.

References

1. Bird AC. X-linked retinitis pigmentosa. *Br J Ophthalmol*. 1975; 59:177–199.
2. Wright AF. Towards the identification of genes in X-linked retinitis pigmentosa. *Prog Ret Res*. 1990;9:197–227.
3. Wright AF, Shu X. Focus on molecules: RPGR. *Exp Eye Res*. 2007;85:1–2.
4. Shu X, Black GC, Rice JM, et al. RPGR mutation analysis and disease: an update. *Hum Mutat*. 2007;28:322–328.
5. Sandberg MA, Rosner B, Weigel-DiFranco C, Dryja TP, Berson EL. Disease course of patients with X-linked retinitis pigmentosa due to RPGR gene mutations. *Invest Ophthalmol Vis Sci*. 2007;48:1298–1304.
6. Fahim AT, Bowne SJ, Sullivan LS, et al. Allelic heterogeneity and genetic modifier loci contribute to clinical variation in males with X-linked retinitis pigmentosa due to RPGR mutations. *PLoS One*. 2011;6:e23021.
7. Cideciyan AV. Leber congenital amaurosis due to RPE65 mutations and its treatment with gene therapy. *Prog Retin Eye Res*. 2010;29:398–427.
8. Jacobson SG, Cideciyan AV, Ratnakaram R, et al. Gene therapy for Leber congenital amaurosis caused by RPE65 mutations: safety and efficacy in 15 children and adults followed up to 3 years. *Arch Ophthalmol*. 2012;130:9–24.
9. Veltel S, Wittinghofer A. RPGR and RP2: targets for the treatment of X-linked retinitis pigmentosa? *Expert Opin Ther Targets*. 2009;13:1239–1251.
10. Jacobson SG, Yagasaki K, Feuer WJ, Román AJ. Interocular asymmetry of visual function in heterozygotes of x-linked retinitis pigmentosa. *Exp Eye Res*. 1989;48:679–691.
11. Beltran WA, Cideciyan AV, Lewin AS, et al. Gene therapy rescues photoreceptor blindness in dogs and paves the way for treating human X-linked retinitis pigmentosa. *Proc Natl Acad Sci U S A*. 2012;109:2132–2137.
12. Hong DH, Pawlyk BS, Shang J, Sandberg MA, Berson EL, Li T. A retinitis pigmentosa GTPase regulator (RPGR)-deficient mouse model for X-linked retinitis pigmentosa (RP3). *Proc Natl Acad Sci U S A*. 2000;97:3649–3654.
13. Chang B, Hawes NL, Hurd RE, et al. Retinal degeneration mutants in the mouse. *Vision Research*. 2002;42:517–525.
14. Hong DH, Pawlyk BS, Adamian M, Li T. Dominant, gain-of-function mutant produced by truncation of RPGR. *Invest Ophthalmol Vis Sci*. 2004;45:36–41.
15. Brunner S, Skosyrski S, Kirschner-Schwabe R, et al. Cone versus rod disease in a mutant Rpgr mouse caused by different genetic backgrounds. *Invest Ophthalmol Vis Sci*. 2010;51: 1106–1115.
16. Wright RN, Hong DH, Perkins B. Misexpression of the constitutive RPGRex1-19 variant leads to severe photoreceptor degeneration. *Invest Ophthalmol Vis Sci*. 2012;52:5189–5201.
17. Aleman TS, Cideciyan AV, Volpe NJ, Stevanin G, Brice A, Jacobson SG. Spinocerebellar ataxia type 7 (SCA7) shows a cone-rod dystrophy phenotype. *Exp Eye Res*. 2002;74:737–745.
18. Jacobson SG, Voigt WJ, Parel JM, et al. Automated light- and dark-adapted perimetry for evaluating retinitis pigmentosa. *Ophthalmology*. 1986;93:1604–1611.
19. Roman AJ, Schwartz SB, Aleman TS, et al. Quantifying rod photoreceptor-mediated vision in retinal degenerations: dark-adapted thresholds as outcome measures. *Exp Eye Res*. 2005; 80:259–272.
20. Araki K, Araki M, Miyazaki J, Vassalli P. Site-specific recombination of a transgene in fertilized eggs by transient expression of Cre recombinase. *Proc Natl Acad Sci U S A*. 1995;92:160–164.
21. Shu X, Simpson JR, Hart A, et al. Functional characterization of the human RPGR proximal promoter. *Invest Ophthalmol Vis Sci*. 2012;53:3951–3958.
22. Aleman TS, Cideciyan AV, Aguirre GK, et al. Human CRB1-associated retinal degeneration: comparison with the rd8 Crb1-mutant mouse model. *Invest Ophthalmol Vis Sci*. 2011; 52:6898–6910.
23. Huber G, Beck SC, Grimm C, et al. Spectral domain optical coherence tomography in mouse models of retinal degeneration. *Invest Ophthalmol Vis Sci*. 2009;50:5888–5895.
24. Knott EJ, Sheets KG, Zhou Y, Gordon WC, Bazan NG. Spatial correlation of mouse photoreceptor-RPE thickness between SD-OCT and histology. *Exp Eye Res*. 2011;92:155–160.
25. Jacobson SG, Aleman TS, Cideciyan AV, et al. Identifying photoreceptors in blind eyes caused by *RPE65* mutations: prerequisite for human gene therapy success. *Proc Natl Acad Sci U S A*. 2005;102:6177–6182.
26. Roman AJ, Boye SL, Aleman TS, et al. Electroretinographic analyses of RPE65-mutant rd12 mice: developing an in vivo bioassay for human gene therapy trials of Leber congenital amaurosis. *Mol Vis*. 2007;13:1701–1710.
27. Cideciyan AV, Jacobson SG. An alternative phototransduction model for human rod and cone ERG a-waves: normal parameters and variation with age. *Vision Res*. 1996;36: 2609–2621.
28. Cideciyan AV. In vivo assessment of photoreceptor function in human diseases caused by photoreceptor-specific gene mutations. *Methods Enzymol*. 2000;316:611–626.
29. Aleman TS, LaVail MM, Montemayor R, et al. Augmented rod bipolar cell function in partial receptor loss: an ERG study in P23H rhodopsin transgenic and aging normal rats. *Vision Res*. 2001;41:2779–2797.
30. Lamb TD, Pugh EN Jr. Phototransduction, dark adaptation, and rhodopsin regeneration: the Proctor Lecture. *Invest Ophthalmol Vis Sci*. 2006;47:5137–5152.
31. Kleinbaum DG, Kupper LL, Nizam A, Muller KE. *Dummy Variables in Regression. Applied Regression Analysis and Other Multivariable Methods, 4th Ed*. Belmont, CA: Duxbury Press; 2007:220.
32. Cheng H, Aleman TS, Cideciyan AV, Khanna R, Jacobson SG, Swaroop A. In vivo function of the orphan nuclear receptor NR2E3 in establishing photoreceptor identity during mammalian retinal development. *Hum Mol Genet*. 2006;15:2588–2602.
33. Cideciyan AV, Rachel RA, Aleman TS, et al. Cone photoreceptors are the main targets for gene therapy of NPHP5 (IQCB1) or NPHP6 (CEP290) blindness: generation of an all-cone Nphp6 hypomorph mouse that mimics the human retinal ciliopathy. *Hum Mol Genet*. 2011;20:1411–1423.
34. Lyubarsky AL, Falsini B, Pennesi ME, Valentini P, Pugh EN Jr. UV and midwave-sensitive cone-driven retinal responses of the

mouse: a possible phenotype for coexpression of cone photopigments. *J Neurosci*. 1999;19:442–455.

35. Walia S, Fishman GA, Swaroop A, et al. Discordant phenotypes in fraternal twins having an identical mutation in exon ORF15 of the RPGR gene. *Arch Ophthalmol*. 2008;126:379–384.
36. Fishman GA, Farber MD, Derlacki DJ. X-linked retinitis pigmentosa. Profile of clinical findings. *Arch Ophthalmol*. 1988;106:369–375.
37. Sharon D, Sandberg MA, Rabe VW. *RP2* and *RPGR* mutations and clinical correlations in patients with X-linked retinitis pigmentosa. *Am J Hum Genet*. 2003;73:1131–1146.
38. Herrera W, Aleman TS, Cideciyan AV, et al. Retinal disease in Usher syndrome III caused by mutations in the clarin-1 gene. *Invest Ophthalmol Vis Sci*. 2008;49:2651–2660.
39. Berson EL, Sandberg MA, Rosner B, Birch DG, Hanson AH. Natural course of retinitis pigmentosa over a three-year interval. *Am J Ophthalmol*. 1985;99:240–251.
40. Birch DG, Anderson JL, Fish GE. Yearly rates of rod and cone functional loss in retinitis pigmentosa and cone-rod dystrophy. *Ophthalmology*. 1999;106:258–268.
41. Iannaccone A, Kritchevsky SB, Ciccarelli ML, et al. Kinetics of visual field loss in Usher syndrome Type II. *Invest Ophthalmol Vis Sci*. 2004;45:784–792.
42. Cideciyan AV, Swider M, Aleman TS, et al. ABCA4 disease progression and a proposed strategy for gene therapy. *Hum Mol Genet*. 2009;18:931–941.
43. Berson EL, Rosner B, Weigel-DiFranco C, Dryja TP, Sandberg MA. Disease progression in patients with dominant retinitis pigmentosa and rhodopsin mutations. *Invest Ophthalmol Vis Sci*. 2002;43:3027–3036.
44. Hosch J, Lorenz B, Stieger K. RPGR: role in the photoreceptor cilium, human retinal disease, and gene therapy. *Ophthalmic Genet*. 2011;32:1–11.
45. Andréasson S, Breuer DK, Eksandh L, et al. Clinical studies of X-linked retinitis pigmentosa in three Swedish families with newly identified mutations in the RP2 and RPGR-ORF15 genes. *Ophthalmic Genet*. 2003;24:215–223.
46. Andréasson S, Ponjavic V, Abrahamson M, et al. Phenotypes in three Swedish families with X-linked retinitis pigmentosa caused by different mutations in the RPGR gene. *Am J Ophthalmol*. 1997;124:95–102.
47. Hoffman DR, Locke KG, Wheaton DH, Fish GE, Spencer R, Birch DG. A randomized, placebo-controlled clinical trial of docosahexaenoic acid supplementation for X-linked retinitis pigmentosa. *Am J Ophthalmol*. 2004;137:704–718.
48. Yagasaki K, Jacobson SG. Cone-rod dystrophy. Phenotypic diversity by retinal function testing. *Arch Ophthalmol*. 1989; 107:701–708.
49. Szamier RB, Berson EL, Klein R, Meyers S. Sex-linked retinitis pigmentosa: ultrastructure of photoreceptors and pigment epithelium. *Invest Ophthalmol Vis Sci*. 1979;18:145–160.
50. Massof RW, Finkelstein D. Vision threshold profiles in X-linked retinitis pigmentosa. *Invest Ophthalmol Vis Sci*. 1979;18:426–429.
51. Demirci FY, Gupta N, Radak AL, et al. Histopathologic study of X-linked cone-rod dystrophy (CORDX1) caused by a mutation in the RPGR exon ORF15. *Am J Ophthalmol*. 2005;139:386–388.
52. Huang Y, Cideciyan AV, Papastergiou GI, et al. Relation of optical coherence tomography to microanatomy in normal and rd chickens. *Invest Ophthalmol Vis Sci*. 1998;39:2405–2416.
53. Jacobson SG, Cideciyan AV, Aleman TS, et al. Crumbs homolog 1 (CRB1) mutations result in a thick human retina with abnormal lamination. *Hum Mol Genet*. 2003;12:1073–1078.
54. Yang Z, Peachey NS, Moshfeghi DM, et al. Mutations in the RPGR gene cause X-linked cone dystrophy. *Hum Mol Genet*. 2002;11:605–611.
55. Jacobson SG, Aleman TS, Cideciyan AV, et al. Defining the residual vision in Leber congenital amaurosis caused by RPE65 mutations. *Invest Ophthalmol Vis Sci*. 2009;50:2368–2375.
56. Aleman TS, Cideciyan AV, Sumaroka A, et al. Inner retinal abnormalities in X-linked retinitis pigmentosa with RPGR mutations. *Invest Ophthalmol Vis Sci*. 2007;48:4759–4765.
57. Thompson DA, Khan NW, Othman MI, et al. Rd9 is a naturally occurring mouse model of a common form of retinitis pigmentosa caused by mutations in RPGR-ORF15. *PLoS One*. 2012;7:e35865.
58. Hong DH, Pawlyk BS, Adamian M, Sandberg MA, Li T. A single, abbreviated RPGR-ORF15 variant reconstitutes RPGR function in vivo. *Invest Ophthalmol Vis Sci*. 2005;46:435–441.
59. Shu X, Zeng Z, Gautier P, et al. Zebrafish Rpgr is required for normal retinal development and plays a role in dynein-based retrograde transport processes. *Hum Mol Genet*. 2010;19: 657–670.